Research Square

Preprints are preliminary reports that have not undergone peer review.
They should not be considered conclusive, used to inform clinical practice,
or referenced by the media as validated information.

Controlling Factors of Post-Fracturing Soaking Time Based on Thermal Recovery in Waxy Shale Oil Reservoirs

Furahieni Yona Mahali
China University of Petroleum (Beijing)
Hakim Ali
hakimbadvi@gmail.com
China University of Petroleum (Beijing)
Hassin Mahtaab
China University of Petroleum (Beijing)
Kato Rutatin Pascraties
China University of Petroleum (Beijing)

Research Article

Keywords: waxy shale oil, soaking time, wax remelting, thermal recovery, hydraulic fracturing, CMG STARS, sensitivity analysis

Posted Date: November 23rd, 2026

DOI: https://doi.org/10.21203/rs.3.rs-11612669/v1

License: This work is licensed under a Creative Commons Attribution 4.0 International License.
Read Full License

Additional Declarations: No competing interests reported.

Controlling Factors of Post-Fracturing Soaking Time Based on Thermal Recovery in Waxy Shale Oil Reservoirs

Furahieni Yona Mahali[a*], Hakim Ali[a,b*], Hassin Mahtaab[c], Kato Rutatin Pascraties[d]

[a]The Unconventional Petroleum Research Institute, China University of Petroleum (Beijing), Beijing 102249, China

[b]State Key Laboratory of Petroleum Resources and Prospecting, China University of Petroleum (Beijing), Beijing, China

[c]College of Petroleum Engineering, China University of Petroleum (Beijing), Beijing 102249, China

[d]State Key Laboratory of Petroleum Resources and Engineering, China University of Petroleum (Beijing), Beijing 102249, China

Corresponding Authors: Furahieni Yona Mahali and Hakim Ali

Abstract:

Hydraulic fracturing in continental lacustrine waxy shale oil formations introduces massive volumes of surface-temperature water into high-temperature rock formations, producing acute localized cooling. In waxy plays such as the Lianggaoshan and Dongyuemiao lacustrine shale formations of the Sichuan Basin, this rapid thermal drawdown cools the near-fracture pore space below the wax appearance temperature (WAT), initiating heavy paraffin crystallization, pore-throat plugging, and severe formation damage. While capillary imbibition and pressure redistribution are typically factored into post-fracturing shut-in schedules, the time needed for geothermal reheating to raise temperatures back above the wax melting point is still not fully understood. A three-dimensional non-isothermal reservoir model was developed in CMG STARS to simulate temperature evolution during cold fracturing fluid injection and subsequent shut-in. The soaking time was determined using a temperature-based criterion, defined as the time required for the monitored temperature to recover above the prescribed wax melting temperature. Near-fracture temperatures fall below the WAT during pumping, and upon shut-in geothermal conduction reheats the invaded zone, driving progressive wax remelting and Temperature recovery. Sensitivity analysis of nine operational, petrophysical, and thermal parameters shows that baseline

formation temperature exerts a dominant control on optimal soaking time (87.7% relative contribution), followed by wax melting temperature (6.9%), porosity (1.7%), and injection fluid temperature (1.5%), whereas injection rate, injection duration, and matrix permeability exert secondary controls (<0.5% each). The amount of thermally optimal soaking time required in all the simulated cases varied from 19.2 hours to 844.8 hours. When evaluating the effect of changing formation temperature on soaking time, it was found that as formation temperature increased from 60°C to 91.5°C, the soaking time decreased from 844.8 hours (35.2 days) to 27.2 hours. At temperatures higher than 80°C, the soaking times were found to be generally between 27 and 37 hours. It was also observed that increasing the temperature of the injected fluid from 5°C to 30°C resulted in a decrease in soaking time from 33.2 hours to 19.2 hours, which is a reduction of 42.2 percent, while holding all other parameters constant. Regression models developed based on each of the sensitivity curves can be used to estimate thermal soaking times based on the parameters examined.

Keywords: waxy shale oil; soaking time; wax remelting; thermal recovery; hydraulic fracturing; CMG STARS; sensitivity analysis

Introduction

There has been a rapid rise in tight and shale oil production that has reshaped global oil supply (Kilian, 2016), and continental shale oil plays have become important strategic targets for unconventional resource development (Eltahan et al., 2021; F. Wang et al., 2021). Continental lacustrine shales, such as the Permian Lucaogou Formation in the Junggar Basin, the Triassic Chang-7 Member in the Ordos Basin, and the Jurassic Lianggaoshan and Dongyuemiao formations in the Sichuan Basin, differ from their marine counterparts in having higher amounts of paraffin wax, which may often exceed 10–20 wt%. Therefore, these lacustrine formations have higher pour points and wax appearance temperatures (WAT) than marine shales (Chen et al., 2022; Li et al., 2015). Long horizontal laterals and multi-stage, high-volume hydraulic fracturing are required to produce these tight formations (J. Wang et al., 2021; Q. Zhang et al., 2022). The design of the stimulation treatment has long been established as an economic decision of first importance for low-permeability reservoirs (Holditch & Tschirhart, 2005). The stimulation of these tight formations utilizes tens of thousands of cubic meters of water-based fracturing fluid, injected at high pump rates (6–15 m^3/min) (Chen et al., 2022; Li et al., 2015; J. Wang et al., 2021).

The extremely low matrix permeability of tight reservoirs has motivated the investigation of enhanced oil recovery (EOR) methods, including both cyclic and conventional water injection, CO_2 huff-n-puff, and miscible gas injection (Manrique et al., 2010; Song & Yang, 2013; Thomas et al., 2014; J. Wang et al., 2018). The fluid exchange between matrix and fractures in these processes is primarily controlled by capillary forces, and as a result, a great deal of research has focused on wettability (Brown & Fatt, 1956; Habibi et al., 2015; Kathel & Mohanty, 2013; D. Wang et al., 2012), spontaneous imbibition tests (Cheng et al., 2019; Dutta et al., 2012; Sun et al., 2022; L. Yang et al., 2018; S. Yang et al., 2019), and imbibition models (Abd et al., 2019; Cai et al., 2014; Khan et al., 2018). Stress-dependent porosity and permeability can further influence matrix-fracture fluid exchange (Teklu et al., 2016).

Field experiments have confirmed the importance of shut-in (soaking) after hydraulic fracturing for post-stimulation performance (J. Wang et al., 2021; Q. Zhang et al., 2022). Previous research has primarily examined capillary-driven spontaneous imbibition, fracture-fluid leak-off dissipation, and the maintenance of reservoir pressure during shut-in (Eltahan et al., 2021; J. Wang et al., 2021). Research on tight and shale oil reservoirs has confirmed that a longer soaking period increases counter-current imbibition, which forces hydrocarbons from the low-permeability matrix into the high-conductivity fractures and reduces aqueous phase trapping (Eltahan et al., 2021; J. Wang et al., 2021; Y. Zhang et al., 2020) have systematically studied the timing of the post-fracturing soak period and showed that well-chosen shut-in timing accelerates hydrocarbon flowback while decreasing early water cut (Chen et al., 2022; J. Wang et al., 2021; Q. Zhang et al., 2022). Related studies on shut-in have focused on many different aspects: water loss during shut-in in gas shales (Makhanov et al., 2014; Yan et al., 2015), the energy-storage and pressure-drop behavior of shut-in schedules (F. Wang et al., 2021), the time-delay effect of imbibition (Y. Zhang et al., 2020), and the optimization of shut-in schedules for various shale plays (Chen et al., 2022; Zhou et al., 2020). Research differentiates multistage fractured well models with embedded discrete fractures and proppant distribution (Yue et al., 2020; Q. Zhang et al., 2020; Zhao et al., 2019) from fracture-propagation studies (Dahi Taleghani et al., 2018), which address a different problem. Unplanned shut-ins, including those during the COVID-19 pandemic, have once again raised awareness of shut-in duration (Jefferson, 2020; Kleit & Taleghani, 2022).

Nonetheless, the existing studies on multi-stage fracturing and shut-in optimization have assumed that the reservoir–fracture system is isothermal (F. Wang et al., 2021; J. Wang et al., 2021; Q.

Zhang et al., 2022). This assumption does not hold true in deep and ultra-deep waxy shale formations (Jiang et al., 2024; S. Yang et al., 2019). Reservoir rocks will typically be between 60 and 150 °C at ambient formation conditions (Jiang et al., 2024; S. Yang et al., 2019). When surface water at 10–25 °C is pumped into a formation in massive volumes, it creates a severe non-isothermal disturbance in the system (Feng et al., 2016; Jiang et al., 2024; S. Yang et al., 2019). Distributed temperature sensing (DTS) and downhole monitoring at the field scale have shown rapid cooling of horizontal wellbores and hydraulic fractures by 30–60 °C within the first few hours of pumping (Jiang et al., 2024; S. Yang et al., 2019). (Feng et al., 2016) showed that thermal drawdown has a substantial effect on local in situ stress fields and fluid rheology.

When a high-wax crude oil meets the lower-temperature invading fracturing fluid, the local temperature drops below the WAT of the oil (Pan et al., 1997; Sandyga et al., 2020). As described by the thermodynamic principles of solid–liquid equilibria and by core-flooding experiments, high-molecular-weight normal alkanes ($>C_{15}$–C_{20}) precipitate out of the crude oil once the temperature drops below its cloud point (Pan et al., 1997). These crystals nucleate, aggregate, and deposit on the rock pore walls and within proppant packs (Pan et al., 1997; Sandyga et al., 2020). (Sandyga et al., 2020) demonstrated through both micro-computed tomography and core-displacement tests that wax crystallization in porous media reduces open porosity by more than 75% and matrix permeability by up to 88%. As the pore throats fill with wax crystals, they form a barrier to fluid flow, an impermeable paraffin skin around the hydraulic fracture face (Sandyga et al., 2020).

Premature reopening of a fractured well before geothermal reheating restores temperature in the cooled near-fracture region above the wax melting threshold. The wax deposits left in the matrix pore throats and proppant packs may restrict fluid flow and impair well productivity (Sandyga et al., 2020).

In contrast, excessively long shut-in periods result in the loss of the elastic energy stored within the fracture system, increase the resistance to water flowback, and extend the capital payback period (Eltahan et al., 2021; J. Wang et al., 2021).

The above reviewed literature highlights a gap in the thermal assessment of post-fracturing soaking time in waxy shale oil reservoirs. Existing shut-in studies primarily emphasize capillary imbibition and pressure redistribution (Chen et al., 2022; Eltahan et al., 2021; F. Wang et al., 2021; J. Wang

et al., 2021; Q. Zhang et al., 2022), while thermal studies of fracturing provide quantitative data on the temperature field around the fracture but do not provide a way to determine the time required to clear wax from the fracture face (Jiang et al., 2024; S. Yang et al., 2019). Studies of wax deposition look at precipitation and the damage it causes, but not at its reversal by geothermal re-warming (Pan et al., 1997; Sandyga et al., 2020). To the best of the authors' knowledge, no study has quantified or ranked the joint effect of operational and reservoir parameters on the length of time required to remelt wax in situ. This motivates systematic assessment of how operational and reservoir parameters influence the thermally required soaking time and their relative importance over specified ranges.

To maximize the recovery of waxy shale oil, it is therefore essential to determine the optimal soaking time on the basis of thermal recovery and in situ wax remelting (Sandyga et al., 2020; J. Wang et al., 2021). To understand the multi-physics of cold fluid invasion, transient heat exchange, wax precipitation, and subsequent geothermal warm-back during post-fracturing shut-in. This study uses CMG STARS to develop a fully coupled, three-dimensional, non-isothermal numerical simulation framework. We utilize the reservoir and fluid databases of the Fuxing shale oil play (Lianggaoshan and Dongyuemiao formations) to examine how the cold zone evolves in time and space, and we then characterize how sensitive the required soaking period is to nine key operational, petrophysical, and thermal parameters.

The main contributions of this study are: (i) a temperature-based definition of the thermally optimal soaking time as the minimum shut-in duration required for the coldest point on the fracture surface to exceed the prescribed wax melting temperature; (ii) a quantitative description of the individual effects of nine operational, petrophysical, and geometrical factors on soaking time, and (iii) a ranking of these factors by their influence on soaking time over the investigated ranges.

2. Methodology

2.1 Research Workflow and Overview

A three-dimensional, non-isothermal reservoir model was developed in CMG STARS to investigate temperature changes during cold-water injection and subsequent shut-in in the Lianggaoshan Formation. The fluid properties were prepared in WinProp and imported into the

reservoir model. The model was then used to simulate the cooling caused by injection and the subsequent temperature recovery during shut-in.

The simulated temperatures were evaluated using the wax appearance temperature (WAT) and wax melting temperature. The WAT of the studied crude oil was 32.38 °C, while a wax melting temperature of 57.92 °C was used for the baseline case. Temperatures below the WAT were considered indicative of conditions favourable for wax precipitation. During shut-in, temperatures were monitored at the fracture surface to determine when the coldest monitored grid block reached the prescribed wax melting temperature.

In this study, the temperature-based optimal soaking time was defined as the elapsed time after shut-in until the coldest monitored fracture-surface grid block reached the wax melting temperature. This criterion represents the minimum simulated shut-in time required to meet the specified thermal condition across the monitored fracture surface.

A series of sensitivity cases was conducted to evaluate the effects of operational, reservoir, fluid, and geometric parameters on the calculated soaking time. The results were compared to assess each parameter's relative influence over its tested range.

Wax precipitation and remelting were interpreted using temperature thresholds; their amounts and rates were not quantified. Similarly, wax-induced permeability impairment was not included in the model.

2.2 Numerical Model and Thermal Evaluation

A three-dimensional, non-isothermal model of the Lianggaoshan Formation was constructed in CMG STARS to examine the temperature response to cold-water injection and subsequent shut-in. Fluid properties were prepared in WinProp and imported into the model. The asphaltene precipitation option was selected during model setup, and a solid phase was defined. However, the analysis focused on the simulated temperature distribution; wax precipitation and remelting were not quantified from the solid-phase output.

The simulation considered two stages: water injection and shut-in. During injection, cold water entered the fracture region and reduced the temperature of the surrounding formation. After injection stopped and the well was shut in, heat transfer from the warmer formation gradually

increased the temperature in the cooled region. The resulting temperature distributions were used to examine the extent of cooling and the subsequent thermal recovery.

The simulated temperatures were compared with the wax appearance temperature and the prescribed wax melting temperature. A temperature below the WAT was taken to indicate conditions under which wax precipitation could occur. During shut-in, the time required for the coldest monitored fracture-surface grid block to reach the melting temperature was used to determine the temperature-based optimal soaking time.

No wax-induced permeability impairment model was included. Therefore, the simulations do not directly establish the amount of wax deposited, the extent of permeability damage, or the degree of productivity recovery after shut-in.

2.3 Definition of the Optimal Soaking Time

The optimal soaking time was determined from the temperature recovery at the fracture surface after injection stopped. In each simulation, the temperatures of the monitored fracture-surface grid blocks were examined during shut-in. The soaking time was taken as the elapsed time from shut-in until the coldest of these grid blocks reached the prescribed wax melting temperature. At this point, all monitored fracture-surface grid blocks had reached or exceeded the threshold.

For the reference case, the melting temperature was set at 57.92 °C. The same procedure was applied to the sensitivity cases, using the prescribed melting temperature for each case. The resulting soaking times were then compared to assess the influence of the selected parameters.

Here, *optimal* refers to the minimum simulated shut-in time needed to meet the temperature criterion. Reaching the melting temperature indicates conditions favourable for wax remelting, but it does not establish how much wax has melted or whether permeability has recovered.

$$t_{soak} = min\{\, t - t_{inj} : T_{f,min}(t) \geq T_{melt}, t \geq t_{inj} \,\} \quad (1)$$

where t is the time since the start of injection, t_{inj} is the injection time, and $T_{\mathrm{f,\,min}}(t)$ is the minimum temperature over the gridblocks of the fracture face at time t. At this instant, the last wax crystals on the fracture face have remelted, so the well can be flowed back without producing through a wax-plugged fracture (Sandyga et al., 2020).

2.4 Sensitivity Analysis Design and Parameter Ranking

A one-at-a-time sensitivity analysis was performed around the baseline case. Each parameter was varied across the range given in Table 1 while all other parameters were kept at their baseline values, and t_{soak} was extracted for every case from Eq. (1). The nine parameters cover the operational (injection rate, injection time, injection fluid temperature), thermal (formation temperature, wax melting temperature), petrophysical (porosity, matrix permeability), and geometric (fracture height, reservoir thickness) controls on soaking.

Table 1 Baseline values and tested ranges of the nine parameters in the one-at-a-time sensitivity analysis.

Parameter	**Unit**	**Baseline**	**Tested range**	**Cases**
Injection rate	m^3/h	174	120–228	8
Injection time	h	1.6	1.0–2.2	7
Formation temperature	°C	85.55	60–91.5	8
Injection fluid temperature	°C	5	5–30	6
Wax melting temperature	°C	57.92	50–70	7
Porosity	–	0.0355	0.0176–0.0705	7
Fracture height	m	74	29–74	6
Reservoir thickness	m	74	37–74	5
Matrix permeability	mD	0.124	0.063-0.230	6

To rank the parameters, the contribution of parameter k to the total variation of the soaking time was computed as

$$C_k = \frac{\Delta t_k}{\sum_{j=1}^{9} \Delta t_j} \times 100\% \quad (2)$$

where $\Delta t_k = |t_{soak,\,max} - t_{soak,\,min}|$ is the absolute change of t_{soak} over the tested range of parameter k, and the sum runs over all nine parameters. Because C_k is based on the range of t_{soak} over each

interval, it depends on the intervals tested, and the percentages should be quoted together with the ranges of Table 1. The ranking is therefore used to distinguish thermal from hydraulic and geometric controls rather than to give absolute importance values.

2.5 Regression Correlations

The relationship between the different variables being studied and the temperature dependent optimal soaking times were described using regression analysis. Each sensitivity series had a curve fitted to its simulated results and the R^2 value was utilized as a measure of how well the fitted curve represented the data points.

The relationship models are used to determine how a single variable will affect the outcome while holding all other variables constant in each series. These models can be used to estimate soaking times for the ranges and conditions tested in each series. However, these models cannot be used together to evaluate what effects may occur when multiple variables change at once, as the potential interactions among them have not been assessed.

2.5.1 Operational parameters

Quadratic equations were fitted to the injection-rate and injection-duration results

$$t_{soak} = -9.0242 \times 10^{-5}\, q^2 + 0.047653\, q + 6.8635 \quad (3)$$

$$t_{soak} = -0.35714\, {t_{inj}}^2 + 2.71429\, t_{inj} + 29.7286 \quad (4)$$

where t_{soak} is the soaking time in hours, q is the injection rate in m³/h, and t_{inj} is the injection duration in hours. The R^2 values were 0.8994 and 0.9663, respectively.

2.5.2 Thermal parameters

Quadratic equations were fitted to the injection-fluid-temperature, formation temperature and wax-melting-temperature results

$$t_{soak} = 0.0100714\, {T_{inj}}^2 - 0.907586\, T_{inj} + 37.3140 \quad (5)$$

$$t_{soak} = 0.176335\, {T_{melt}}^2 - 18.08328\, T_{melt} + 487.4412 \quad (6)$$

$$t_{soak} = 2016.94(T_f - 57.92)^{-1.12291} \quad (7)$$

where T_{inj} is the injection-fluid temperature and T_{melt} is the prescribed wax melting temperature, both in °C. The R^2 values were 0.9973 and 0.9902, respectively, while for the T_f , $R^2 = 0.9706$

2.5.3 Petrophysical and geometric parameters

For porosity, φ (fraction), the three simulated points are described by a linear relation, and for fracture height, h_f (m), and reservoir thickness, h_r (m), by quadratic relations:

$$t_{soak} = 570.2172\,\varphi + 12.2076 \quad (8)$$

$$t_{soak} = 0.00181324\,{h_f}^2 - 0332448\,h_f + 47.4356 \quad (9)$$

$$t_{soak} = 0.00299312\,{h_r}^2 - 0.443940\,h_r + 49.7648 \quad (10)$$

with $R^2 = 0.9791$ for Eq. (9), 0.9818 for Eq. (10), and 0.9944 for Eq. (8). No correlation is given for matrix permeability, whose effect on t_{soak} is negligible (Section 4.4.3).

2.5.4 Range of validity

Equations (3)– (10) are summarized in Table 2, and in all of them t_{soak} is in hours. They describe the local sensitivity of t_{soak} to one parameter at a time, with all others at their baseline values, so they must not be added or multiplied to predict a case in which several parameters change together. They are valid only within the ranges of Table 2 and should not be extrapolated. Eq. (7) shows the largest scatter at the lowest formation temperatures (60–62 °C), where t_{soak} is most sensitive to the thermal margin. A single multi-parameter design correlation would require a common baseline and an independent validation set, which are not part of this study.

Table 2 Regression correlations of the optimal soaking time: fitted range, number of cases, functional form, and coefficient of determination.

Parameter	Fitted range	Cases	Form	Equation
Injection rate	120–228 m³/h	8	Quadratic	(3)
Injection time	1.0–2.2 h	7	Quadratic	(4)
Formation temperature	60–91.5 °C	8	Power law	(7)
Injection temperature	5–30 °C	6	Quadratic	(5)

Parameter	Fitted range	Cases	Form	Equation
Wax melting temperature	50–70 °C	7	Quadratic	(6)
Porosity	0.0176–0.0705	7	Linear	(8)
Fracture height	29–74 m	6	Quadratic	(9)
Reservoir thickness	37–74 m	5	Quadratic	(10)

3. Reservoir Characterization and Simulation Setup

3.1 Geological Setting: Fuxing Lacustrine Shale Oil Play

The Fuxing shale oil area, located in the eastern Sichuan Basin, represents a major continental lacustrine tight shale play. The target intervals comprise the Jurassic Lianggaoshan Formation and the Dongyuemiao Member of the Ziliujing Formation. These units are characterized by interbedded organic-rich black shales, silty mudstones, and tight argillaceous siltstones deposited deep into semi-deep lacustrine environments. The matrix system possesses ultra-low permeability (0.001–0.1 mD) and low porosity (2.0–7.5%), with micro- and nanoscale pore throats dominating the storage space (Chen et al., 2022).

Crude oils produced from the Lianggaoshan and Dongyuemiao intervals are paraffinic, featuring high wax contents (12.0–22.5 wt%), high stock-tank pour points (22–36 °C), and high downhole wax appearance temperatures (55–72 °C) (Pan et al., 1997; Sandyga et al., 2020). Virgin reservoir temperatures range from 65 °C in shallower sections to over 95 °C in deeper zones, under normal-to-high pressure gradients (1.2–1.6 MPa/100 m) (Chen et al., 2022; J. Wang et al., 2021). Because the reservoir temperature is only 10–25 °C above the crude's WAT, cold water injection creates severe localized paraffin crystallization.

3.2 Computational Domain and Numerical Discretization

To simulate the physical processes of multi-stage hydraulic fracturing, a 3D reservoir model representing a single fracture stage and single perforation cluster was constructed in CMG STARS. The computational grid employs logarithmic local grid refinement (LGR) orthogonal to the

fracture plane to resolve the steep pressure, temperature, and saturation gradients that develop across the hydraulic fracture face.

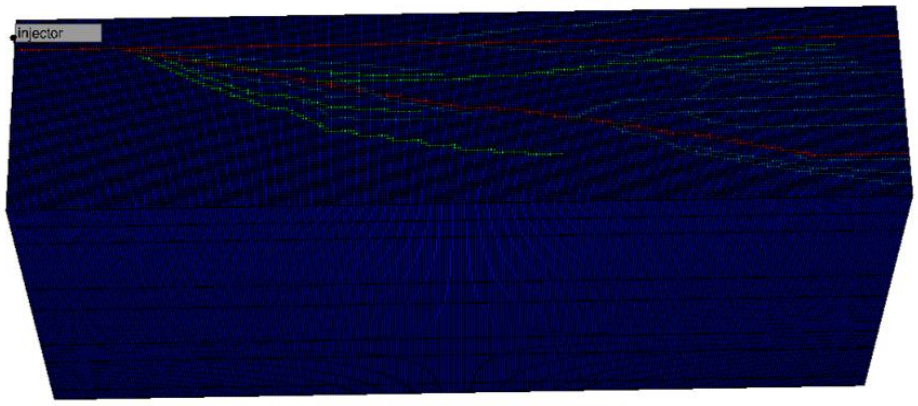


Figure 1 Three-dimensional reservoir model showing injector location, hydraulic fracture geometry, and computational grid.

A three-dimensional Cartesian model was constructed with dimensions 160 m × 36 m × 74 m along the *x*-, *y*-, and *z*-directions, respectively. The domain was discretized into 320 × 72 × 8 grid cells with uniform horizontal spacing of 0.5m and vertical layer thicknesses of 6, 6, 17,8,14,7,12 and 4m. Layer-dependent matrix porosity and horizontal permeability ranged from 0.0315 to 0.0395 and from 0.10 t0 0.14mD, respectively. The fracture network comprised main and subsidiary branches represented by elevated permeability cells extending through all eight layers. An injection well connected to the fracture network was completed through these layers at a fixed horizontal location. The reservoir was initialized at a uniform temperature of 85.55 °C and a pressure of 39Mpa. Water at 5 °C was injected under a minimum surface rate of 174 m^3/h for 1.6 h, followed by well shut-in to evaluate temperature recovery.

4 Results and Discussion

4.1 Cooling During Injection and Thermal Recovery During Shut-In

The cold-fluid injection produces a spatially non-uniform thermal disturbance in the fractured reservoir. Temperature distribution on the horizontal reservoir plane is shown in Figure 2 during the cold fluid injection. Relative to the initial temperature of 85.55°C, cold fluid (water) injected at 5°C cools the fractured reservoir along the fractures. Distribution of the cooled regions depends

upon the fracture geometry, which is used as input into the model. The fractures serve as preferential flow paths for moving the cold injected fluid through the formation. On the other hand, areas located away from the cold-fluid flow paths are relatively warmer; hence, the thermal disturbance caused by the cold-fluid injection is concentrated in the area of the cold-fluid-invaded fracture network.

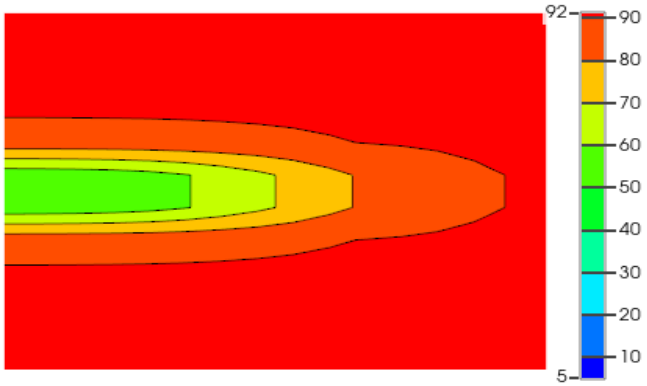


Figure 2 Evolution of the temperature distribution in the horizontal reservoir plane (I–J view) during the injection time

The temperature differences that exist in the vicinity of fractures relative to the surrounding matrix are indicative of the differing ways in which moving water transports thermal energy and how it interacts with the adjacent rock and/or reservoir fluids. Fluid movement through the higher permeability fracture network transports the thermal effects generated by the injection process away from the fractures, while transferring thermal energy to the adjacent rock and/or reservoir fluids. Therefore, the area affected by cooling extends into the surrounding matrix; however, the extent of the area being cooled will depend upon how long moving water is injected and what are the specific thermal and hydraulic characteristics of the site. The fact that areas of increased temperature continue to persist at a distance from the fractures indicates that the reservoir has not been cooled uniformly and that the surrounding rock continues to retain thermal energy that can be used to heat up the area again in the future.

This temperature distribution allows us to locate areas that may be at risk for wax precipitation in waxy crude oils. We assume that if the simulated temperature drops below the stated wax appearance temperature, then wax will precipitate as per the temperature-based interpretation used.

Figure 2 therefore indicates where conditions are such that precipitation can occur but does not provide an indication of how much wax was deposited nor how it affected fluid flow.

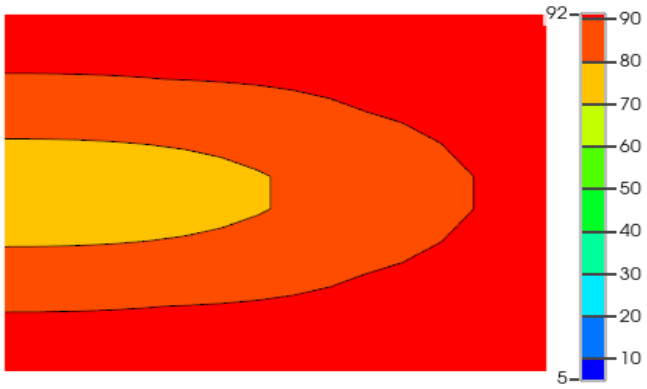


Figure 3 Evolution of the temperature distribution in the horizontal reservoir plane (I–J view) during soaking time

Shut-in is followed by cessation of cold-water flow to the fractured region, and cooling of the fractured region reverses due to heat transfer from the warmer surrounding formation. As illustrated in Figure 3, temperature increases in regions which had been cooled during injection. A comparison of Figures 2 and 3 indicates that the thermal disturbances caused by cold-water injection are reversed after shut-in: cold-water flow into the fracture network was the primary mechanism of cooling during injection; however, after shut-in, cold-water flow stops, and heat flows from the warmer rock adjacent to the fracture network into the fracture network.

The spatial distribution of recovery is non-uniform due to the varying rates of cooling in the various portions of the fracture system as well as the varying local heat transfer characteristics. Thus, while an increase in the mean reservoir temperature may suggest that some portion of the fractured area has reached the remelting criteria, it cannot be assumed that all such areas have done so. Therefore, the lowest temperature on the observed fracture face will be used to define the optimum thermal soaking time. This time is the shortest amount of shut-in time required for that location to reach the required wax melting temperature.

Under this definition, full recovery of original reservoir temperatures is not needed; rather, the appropriate goal is to achieve the specified melting point along the entire monitored fracture surface. Thermal conditions indicate wax melting has occurred; however, removal of solid wax and recovery of permeability are not explicitly measured. Consequently, Figures 2 and 3 provide

the thermal basis for conducting a subsequent sensitivity analysis to determine how changes in reservoir and/or operational characteristics impact the duration of time needed to meet this standard.

4.2 Impact of Operational Parameters on Optimal Soaking Time

4.2.1 Effect of Injection Rate

Figure 4 demonstrates how the injection rate impacts the optimal thermal soaking time in the Lianggaoshan Formation, given that the injection rates ranged from 120 to 228 m³/h. In each simulation, the injection time was held constant at 1.2 h, the injected fluid temperature at 5°C, the initial reservoir temperature at 85.55°C, and the wax melting temperature at 57.92°C, while the remaining model parameters were not modified. Within the specified range of injection rates, the soaking time consistently increased from 31.36 to 33.00 hours. Therefore, a 90% increase in injection rate resulted in an additional thermal recovery requirement of 1.64 hours, which is approximately a 5.23% increase.

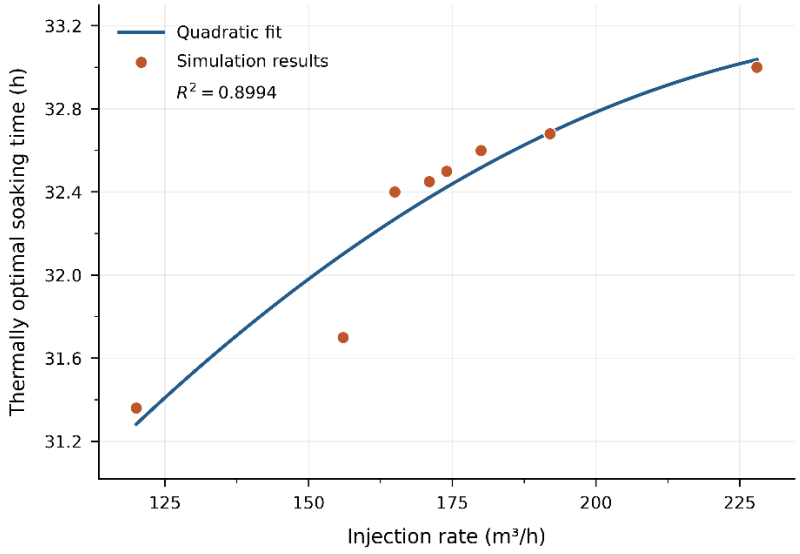


Figure 4 Sensitivity of optimal soaking time to injection rate variation, demonstrating the nonlinear relationship between injection intensity and the required soaking duration for wax remelting.

The duration of the injection was held constant; therefore, as the rate increased, the amount of injected water also increased from 144 m³ to 273.6 m³. An increased amount of cold water

introduced to the fracture/matrix system creates a larger thermal disturbance, which is reflected in a longer recovery period. There was a very small difference in the soaking time. This suggests that under these experimental conditions, the thermal end point did not respond significantly to changes in the injection rate. Therefore, this comparison reflects the effects of changing the injection rate while keeping the duration of the injection the same; it also reflects the effect of changing the volume of injected water.

A quadratic model fits the data well ($R^2 = 0.8994$). While the model indicates that soaking time increases at decreasing rates as flow rate increases, the eight simulated cases do not allow for the determination of a limiting value or the mechanism that controls it. Additionally, there are two areas where the data departs from the trend established by the model. First, there is a relatively small change in soaking time from 120 m^3/h to 156 m^3/h. Secondly, there is a much greater change in soaking time from 156 m^3/h to 165 m^3/h. It is possible that these differences in soaking times could be due to numerical errors; however, additional evidence would be required to support this claim.

From an operational point of view, the injection rate of fluid used during fracturing has very little influence on determining the thermally optimal soaking time that should be used for fracturing in order to achieve the best results. The maximum rate of injection examined in this study had a net increase in the length of time needed to shut in the well of only 2 hours as compared to the minimum rate. This result is based upon the given injection period and the type of reservoir configuration that was studied. It does not determine which injection rate would be most effective for fracturing or for increasing the total production from a well.

4.2.2 Effect of Injection Duration

Figure 5 illustrates how the amount of time that a well is shut in after being injected with fluid affects the thermal optimum in soaking time. At a fixed injection rate of 174 m^3/h, as the amount of time the fluid is injected into the well is increased from 1.0 hour to 2.2 hours, the amount of time that the fluid needs to remain shut-in increases from 32.0 hours to 34.1 hours. This represents

an increase of 2.1 hours, or 6.56%. For the duration of injection investigated, there appeared to be a relatively linear relationship between the two variables ($R^2 = 0.9603$).

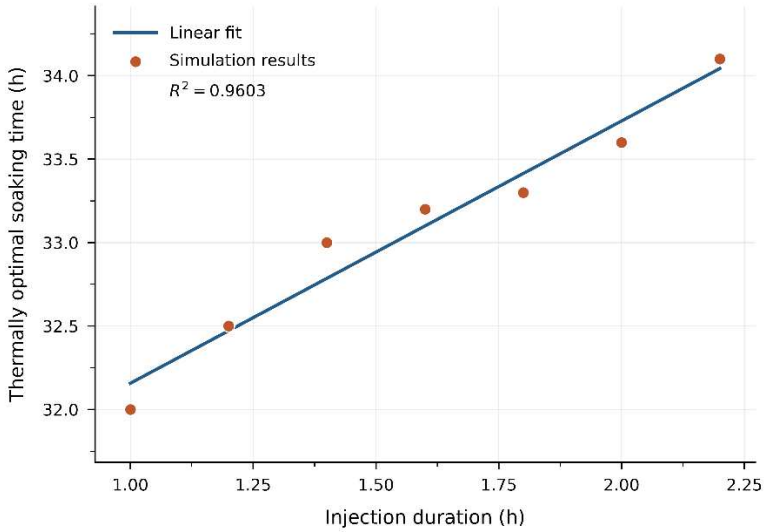


Figure 5 Sensitivity of optimal soaking time to injection time variation, demonstrating the nonlinear relationship between injection intensity and the required soaking duration for wax remelting.

Under this protocol, longer injection times will lead to more extended periods of cold-fluid contact as well as a larger total amount of fluid being introduced into the fracture, which creates a larger thermal perturbation than shorter injection protocols. Therefore, the longer injection time leads to a longer period of thermal disturbance before the temperature of the fracture reaches the predetermined melting point. However, although there was a slight increase in soaking time, it is apparent that there is little dependence of soaking time upon injection duration under the parameters of this study. The larger volume of fluid introduced during the longer injection protocol from 174 m^3 to 382.8 m^3 indicates that the increased soaking time experienced with the longer injection protocol can be attributed to both the longer exposure to cold fluid as well as to the

increased amount of fluid added to the system; therefore, it cannot be said that the preferred injection time can be determined based on a fixed treatment volume.

4.3 Impact of Thermal Parameters on Optimal Soaking Time

4.3.1 Effect of Initial Formation Temperature

Initial formation temperature represents the internal geothermal heat store available to warm the invaded fracture zone. As formation temperature increases from 60 to 91.5 °C, the optimal soaking time drops nonlinearly from 844.8 h (over 35 days) to 28.8 h (Figure 6). When ambient temperature is close to the wax melting temperature (57.92 °C), a very small thermal gradient requires an extended shut-in to remelt precipitated wax. Conversely, in deeper, hotter formations (>80 °C), large conductive thermal gradients drive rapid warm-back within 30–40 h, which is a high soaking time.

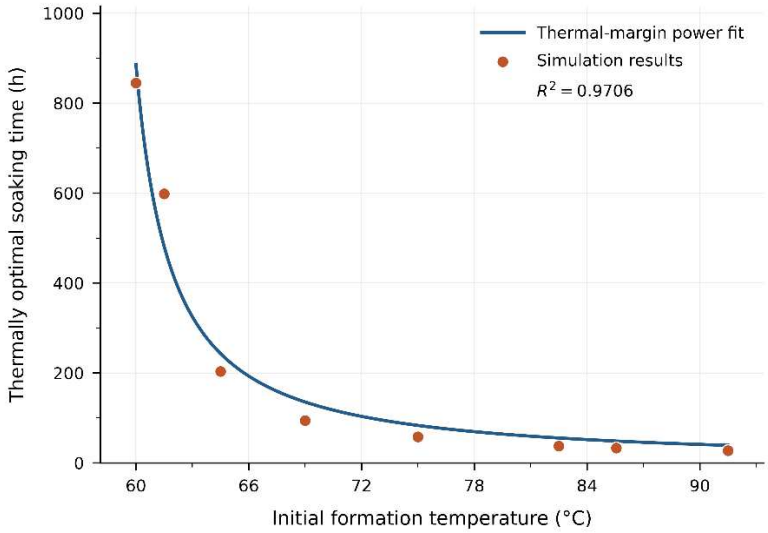


Figure 6 Influence of formation temperature on the optimal soaking time for wax remelting, showing the nonlinear reduction of required soaking duration with increasing reservoir temperature.

This is the most important result of the study. The soaking time falls by a factor of almost 31 over a 31.5 °C change in formation temperature, and the curve is steepest at the cold end, as observed from 60 to 64.5 °C, it reduced soaking time by 75.9% (844.8 h to about 203.4 h), whereas increasing it from 82.5 to 91.5 °C shortened soaking time by only 26% (10.1 h). In the tested cases, margins above 20 °C allow flowback after roughly 1.5–2 days, whereas the two cases with margins

below 5 °C require more than a week. These results indicate the substantial shut-in requirement associated with formation temperatures close to the wax melting threshold.

4.3.2 Effect of Injection Fluid Temperature

Increasing the injected fluid temperature from 5 to 30°C shows a negative effect on the soaking time. It decreased from 33.2 to 19.2 hours (a decrease of 14.0 hours, or 42.2%), as shown in Figure 7. Considering the condition that formation temperature, wax melting temperature, injection rate, and injection duration remained unchanged during all experiments at 85.55°C, 57.92°C, 174m^3/hr and 1.6 hrs, respectively. Figure 7 illustrates that there are diminishing returns associated with increasing fluid temperature. The difference in soaking time between injecting fluid at 5°C versus 10°C was 4.37 hours. However, the difference in soaking time when injecting fluid at 25°C versus 30°C was only 1.47 hours. This trend can be mathematically represented using a second-order polynomial function with an R^2 value of 0.9973.

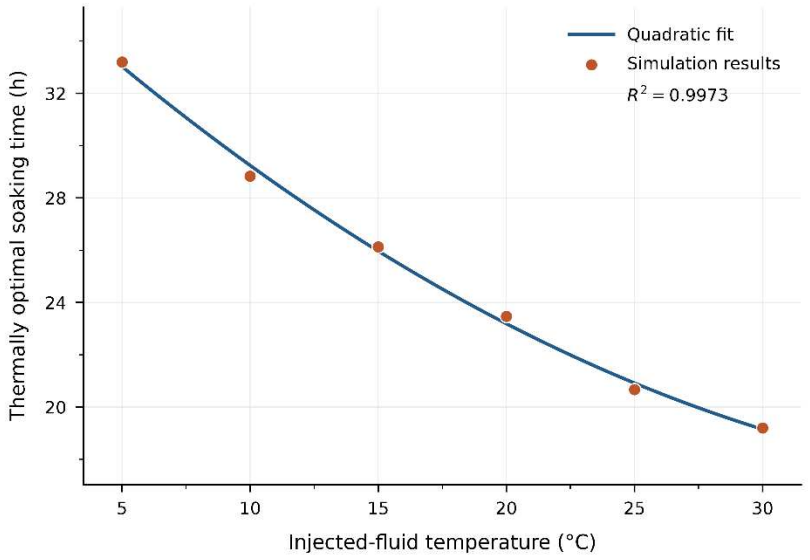


Figure 7 Influence of injection temperature on the optimal soaking time for wax remelting, showing the nonlinear decrease in required soaking duration with increasing injection temperature.

The lower the temperature difference between the injected water and the reservoir, the less cooling occurs during the injection process. As such, the amount of thermal recovery required to reach the wax melting point is reduced. Therefore, injecting cooler water results in a longer shut-in period; conversely, increasing the temperature of the injected water will result in a shorter shut-in period.

For all studied cases, the effects of warming the injected water had significantly larger impacts on soaking time than did the effects of both injection rates (which affected soaking times by only 1.64 hours) and injection durations (which affected soaking times by only 2.10 hours); however, the effects of warming the injected water were much less significant than the effects of formation temperatures. Thus, although energy requirements and economic benefits were not assessed, it is recommended that consideration be given to warming injected water to reduce thermal shut-in delays.

4.3.3 Effect of Wax Melting Temperature

The wax melting point (T_{melt}) defines the thermal target needed to clear wax blockages. Higher melting thresholds demand greater geothermal reheating, causing the required soaking duration to increase nonlinearly from 24 h at T_{melt} = 50 °C to 88.8 h at T_{melt} = 70 °C. Crudes with higher fractions of heavy C_{35+} alkanes possess higher melting points, requiring significantly extended shut-in periods to ensure complete pore-throat cleanout (Pan et al., 1997; Sandyga et al., 2020)

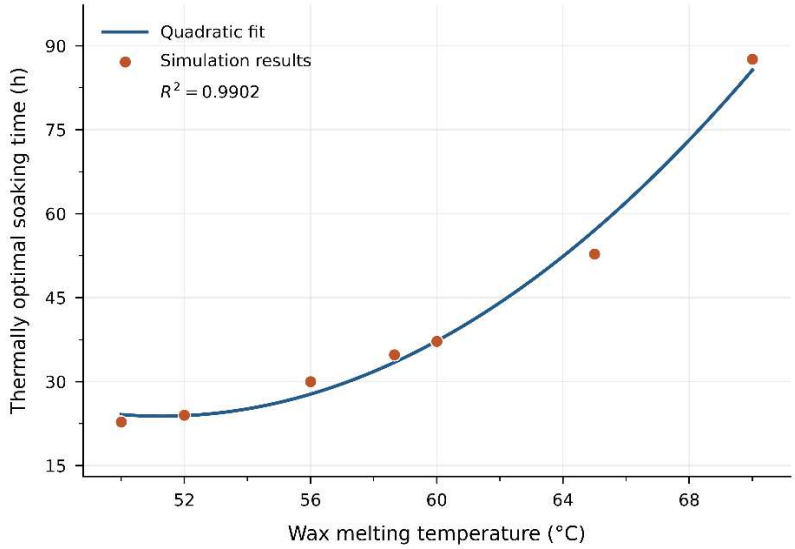


Figure 8 Influence of wax melting temperature on the optimal soaking duration, demonstrating the increasing thermal recovery time required for remelting wax with higher melting thresholds.

The soaking time increases by a factor of 3.84 over the 20 °C range, and the increase accelerates, the first 10 °C (50 to 60 °C) add about 14.4 h, the second 10 °C about 50.4 h, i.e. about 1.44 h/°C near 50 °C but about 5.04 h/°C near 70 °C, because the margin to the reservoir temperature (85.55 °C) shrinks as the target rises. The response is steeper than the margin alone would suggest,

so latent heat for remelting, likely larger for crudes that form more wax, may also contribute; this could be tested with latent heat set to zero. Because the melting temperature is a measurable crude property, a good estimate of it is far more valuable for planning the soak than a refined injection rate, whose effect is about 39.5 times smaller over the tested ranges (1.65 h against 64.8 h).

4.4 Impact of Petrophysical and Geometric Properties on Optimal Soaking Time

4.4.1 Effect of Reservoir Porosity

Porosity affects the amount of pore space in which fluids may be stored, likewise for the fluid-to-rock ratio involved in thermal exchange. This can affect how the fluid is redistributed, how far the area is cooled, and how quickly the same area is reheated. The fact that the porosity increased over time suggests that the cases with higher porosity took longer to reach temperatures greater than the melting point. Because water has a higher volumetric heat capacity (≈4.18 MJ/m^3·°C) than dry rock minerals (≈2.35 MJ/m^3·°C), formations with greater porosity will store a larger volume of cold water per unit of rock volume. Higher-porosity formations will therefore have a larger overall thermal deficit, which creates longer soaking time from 21.4 h at $\varphi = 0.0176$ to 51.2 h at $\varphi = 0.0705$ (Figure 9). Formations with higher storage capacity can absorb a greater volume of cold water, thus creating a larger heat sink and slowing the rate of geothermal reheating. However, the soaking-time results alone cannot separate these mechanisms or attribute the response solely to increased heat capacity.

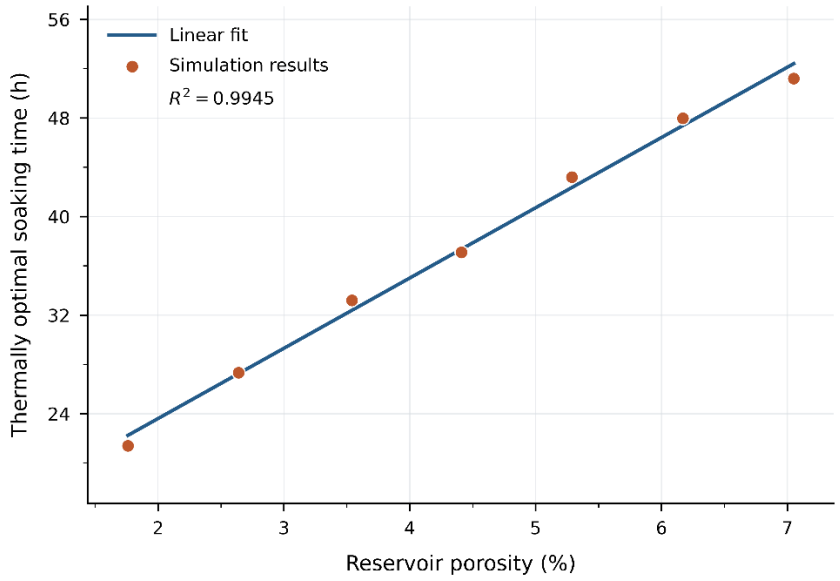


Figure 9 Influence of reservoir porosity on the optimal soaking time for wax remelting, showing the increase in required soaking duration with increasing pore volume.

Across the studied limits, porosity affected the amount of soaking time by 29.8 hours. This change was greater than the change due to the injection rate, injection duration, and injected-fluid temperature; however, it was less than the change resulting from the formation temperature and the melting threshold. Therefore, porosity can be used as a significant constraint for reservoirs when determining thermal shut-in requirements, and this relationship is based upon the tested range and configuration.

4.4.2 Effect of Fracture Height and Reservoir Thickness

Both parameters show a negative correlation with soaking time. For example, as the fracture height increases from 29 to 70 m, the required soaking time decreases from 40.9 to 34.0 h (Figure 10a). Likewise, as the reservoir thickness increases from 37 to 70 m, the soaking duration decreases from 39.0 to 35.1 h (Figure 10b). The larger the vertical contact area, the more quickly heat can be conducted vertically from the hot overlying and underlying confining beds, thus speeding up thermal recovery along the fracture face. At a fixed injected volume, a taller fracture may distribute cold fluid over a larger contact area, reducing cooling intensity per unit area, while a thicker reservoir increases the rock volume available for heat storage and exchange.

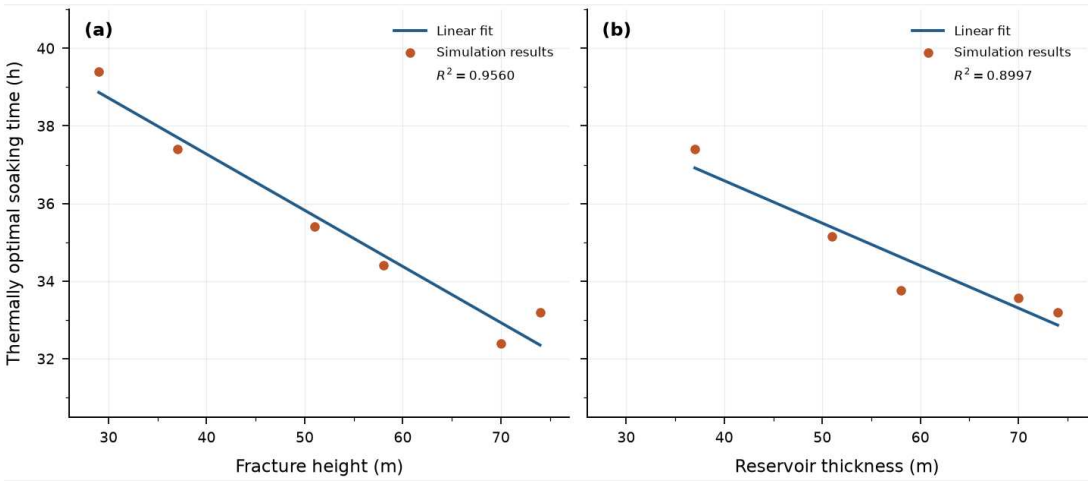


Figure 10. *Sensitivity of thermally optimal soaking time to (a) fracture height and (b) reservoir thickness*

Geometric parameters have only a slight influence: soaking time decreases by approximately 17.8% between 29 and 70 m of fracture height (about 0.171 h/m), and by approximately 10.2% between 37 and 70 m of reservoir thickness (about 0.116 h/m). Fracture height has a greater effect than injection rate (6.9 h against 1.64 h), but both have a smaller effect than the thermal parameters outlined in Section 4.3, which makes them better suited to act as screening parameters than as optimization variables.

4.4.3 Effect of Matrix Permeability

A small variation in thermally optimal soaking times was observed, and there was an erratic change in trends for optimal soaking times when the matrix permeability increased from 0.063 mD to 0.230 mD. For example, the optimal duration was as short as 30.4 hours (at 0.157 mD) and as long as 33.55 hours (at 0.230 mD), giving a total difference of only 3.15 hours. At a baseline permeability of 0.124 mD, the required soaking time was found to be 33.2 hours. Matrix permeability does not have a linear relationship with soaking duration, unlike other variables like porosity and thermal properties.

Permeability directly affects how cold fluids enter a reservoir and subsequently redistribute throughout the reservoir, therefore affecting the rate at which cold fluid cools down a reservoir. Due to the very small differences in the most effective soaking time periods for each case study, it can be concluded that permeability has less effect on thermal recovery criteria than geologic and

geometrical parameters. However, when comparing permeability effects on thermal recovery to operational variables (such as injection rate and injection duration), permeability has a greater effect on thermal recovery.

The descriptive quadratic model proposed has poor predictive ability since it has a very small coefficient of determination ($R^2 = 0.3081$). Therefore, the descriptive quadratic model can't be used to estimate a reliable correlation and therefore can't be used to determine an appropriate permeability threshold. Additional modeling and strict convergence analysis must occur in order to explain why some of the results from the simulation were so irregular.

5. Global Sensitivity Analysis and Parameter Ranking

To evaluate the relative influence of all examined factors, a range-based comparison of the one-at-a-time simulation suite was performed. Figure 12 presents the tornado diagram displaying the percentage contribution of each parameter.

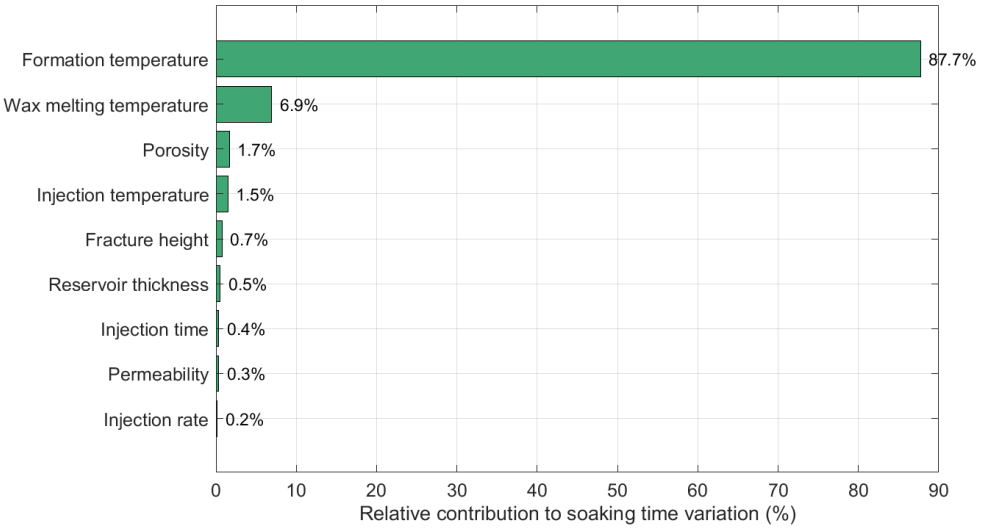


Figure 12 Relative contribution of the nine parameters to the variation of the optimal soaking time (tornado diagram).

The global sensitivity ranking confirms that thermal conditions dominate soaking duration. Baseline formation temperature accounts for 87.7% of the total variation, while wax melting temperature contributes 6.9%. Petrophysical porosity and operational injection fluid temperature provide secondary contributions of 1.7% and 1.5%, respectively. Fracture height (0.7%), net

reservoir thickness (0.5%), injection duration (0.4%), matrix permeability (0.3%), and injection rate (0.2%) exert minor controls.

Table 3 Tested range of each parameter and the corresponding minimum and maximum optimal soaking time.

Parameter	Tested range	Cases	tsoak at start of range (h)	tsoak at end of range (h)
Formation temperature	60–91.5 °C	8	844.8	27.2
Wax melting temperature	50–70 °C	7	22.8	87.6
Porosity	0.0176–0.0705	7	21.4	51.2
Injection temperature	5–30 °C	7	33.2	19.2
Fracture height	29–74 m	6	39.4	33.2
Reservoir thickness	37–74 m	5	37.4	33.2
Injection time	1.0–2.2 h	7	32	34.1
Injection rate	120–228 m^3/h	8	31.36	33
Permeability	0.063–0.230	6	32.4	33.55

6. Discussion

6.1 Engineering Implications

The results suggest that the difference between initial formation temperature and wax melting temperature is an important consideration when estimating thermal recovery during shut-in. In the formation-temperature sensitivity series, a small temperature difference was associated with a much longer time for the coldest monitored fracture-surface grid block to reach the melting threshold. For the tested cases, differences above approximately 20 °C corresponded to soaking times of about 27–37 h, whereas differences below 5 °C corresponded to times exceeding 24 days. These values are specific to the Lianggaoshan model and the conditions used in that series.

An appropriate estimate of the crude-oil melting temperature is also important. In the melting-temperature sensitivity series, increasing the prescribed threshold from 50 to 70 °C increased the

calculated soaking time from 22.8 to 87.6 h. Injection-fluid temperature also influenced the result: increasing it from 5 to 30 °C reduced soaking time from 33.2 to 19.2 h under the conditions tested.

The calculated soaking time provides a temperature-based criterion for assessing shut-in duration. It indicates when the monitored fracture surface has reached the prescribed melting temperature; it does not confirm that wax removal or permeability recovery is complete. In practice, shut-in planning may also need to consider other objectives, including imbibition and pressure redistribution, alongside operational and economic constraints.

6.2 Comparison with Previous Work

Previous studies have examined shut-in duration in relation to processes such as fluid imbibition and pressure redistribution in fractured tight reservoirs (Chen et al., 2022; F. Wang et al., 2021; J. Wang et al., 2021; Q. Zhang et al., 2022). The present study adds a thermal perspective by estimating the time required for the cooled fracture surface to reach a prescribed wax melting temperature.

Over the tested Lianggaoshan ranges, formation temperature and the prescribed melting temperature produced larger changes in calculated soaking time than matrix permeability. This comparison is specific to the parameter ranges and reference conditions used in the sensitivity analysis. It does not establish that thermal recovery is independent of fluid redistribution or other shut-in processes.

The potential for wax deposition and associated formation damage has been discussed in previous work, including (Sandyga et al., 2020). In the present study, however, wax deposition and damage were not quantified; the results indicate thermal conditions relevant to wax behaviour. A comparison with measured temperature-recovery data would be valuable for assessing the model's ability to represent field behaviour.

6.3 Limitations and Future Work

The study contains some limitations; one limitation is that the results are based on a numerical representation of the Lianggaoshan Formation; therefore, the applicability of the results to other formations and fracture configurations is unknown. A second limitation of the study was the sensitivity analysis. Sensitivity analysis varied each parameter separately and did not evaluate

interactions between parameters. Additionally, the magnitude and order of the effect of each parameter depend upon the range of values used.

Thirdly, soaking time was determined based on when the coldest fracture-surface grid block reached a specified temperature. The amount of wax precipitated, the rate of wax melting, how much permeability was reduced by the wax, and how quickly permeability recovered from the reduction caused by the wax were all unmeasured. Therefore, once the specified temperature is reached, it cannot be assumed that all wax has been removed. Lastly, the model used in this study and the regression equations derived from it must be tested against additional independent data sets.

Future research should involve comparing simulated temperature recovery to actual downhole measurements. Also, a larger number of sensitivity studies should be conducted so that we may better understand the interaction between various parameters. If appropriate fluid and rock data are available, then a wax deposition/permeability impairment model can be used to determine the relationship between temperature recovery, wax removal, and the performance of the well.

7. Conclusions

This study used a three-dimensional, non-isothermal CMG STARS model of the Lianggaoshan Formation to examine temperature changes during cold-water injection and subsequent shut-in. A temperature-based optimal soaking time was defined as the time required after shut-in for the coldest monitored fracture-surface grid block to reach the prescribed wax melting temperature. The sensitivity analysis led to the following conclusions:

1. Formation temperature had the largest effect over the tested ranges**.** Increasing it from 60 to 91.5 °C reduced the calculated soaking time from 844.8 to 27.2 h. The increase in soaking time was particularly pronounced when formation temperature was close to the prescribed melting temperature.
2. The prescribed wax melting temperature also strongly influenced the result. Increasing the threshold from 50 to 70 °C increased the calculated soaking time from 22.8 to 87.6 h. This finding highlights the importance of selecting an appropriate melting temperature for the crude oil when applying the thermal criterion.

3. Injection-fluid temperature and porosity had notable effects**.** Increasing injection-fluid temperature from 5 to 30 °C reduced soaking time from 33.2 to 19.2 h, while increasing porosity from 0.0176 to 0.0705 increased it from 21.4 to 51.2 h.
4. Injection rate, injection duration, fracture height, reservoir thickness, and matrix permeability produced smaller changes in soaking time over their respective tested ranges**.** The ranking is specific to the parameter ranges and reference conditions used in this study.
5. The proposed criterion provides a way to assess thermal recovery during shut-in. Reaching the melting threshold indicates conditions favourable for wax remelting, but the simulations did not quantify wax removal or permeability recovery. Further comparison with measured temperature-recovery data and simulations that account for wax deposition and damage would help assess its practical application.

The fitted regression equations describe the individual sensitivity trends within the tested ranges. They should not be used to predict the combined effects of changing several parameters without further validation.

CRediT authorship contribution statement

Furahieni Yona Mahali: Data curation, Methodology, Software, Formal analysis, Visualization, Writing – review & editing.

Hakim Ali: Conceptualization, Formal analysis, Writing – original draft, Writing – review & editing.

Hassin Mahtaab: Writing – review & editing.

Kato Rutatin Pascraties: Writing – review & editing.

Declaration of competing interests

The authors declare that they have no known competing financial interests or personal relationships that could have appeared to influence the work reported in this paper.

Data availability

The reservoir and fluid properties and simulation results selected for reporting are presented in this article. The underlying field data and simulation model files are confidential and are not publicly available.

Declaration of generative AI and AI-assisted technologies

During the preparation of this work, the authors used generative AI and AI-assisted tools to improve language and readability. After using these tools, the authors reviewed and edited the content as needed and take full responsibility for the content of the publication**.**

References

1. Abd, A. S., Elhafyan, E., Siddiqui, A. R., Alnoush, W., Blunt, M. J., & Alyafei, N. (2019). A review of the phenomenon of counter-current spontaneous imbibition: Analysis and data interpretation. *Journal of Petroleum Science and Engineering*, *180*, 456–470. https://doi.org/10.1016/j.petrol.2019.05.066
2. Brown, R. J. S., & Fatt, I. (1956). Measurements Of Fractional Wettability Of Oil Fields' Rocks By The Nuclear Magnetic Relaxation Method. *Fall Meeting of the Petroleum Branch of AIME*, SPE-743-G. https://doi.org/10.2118/743-G
3. Cai, J., Perfect, E., Cheng, C.-L., & Hu, X. (2014). Generalized Modeling of Spontaneous Imbibition Based on Hagen–Poiseuille Flow in Tortuous Capillaries with Variably Shaped Apertures. *Langmuir*, *30*(18), 5142–5151. https://doi.org/10.1021/la5007204
4. Chen, X., Liao, K., Lv, Z., Zhu, J., Wang, J., Li, Y., & Wang, F. (2022). Numerical Simulation Study on Optimal Shut-In Time in Jimsar Shale Oil Reservoir. *Frontiers in Energy Research*, *10*, 849064. https://doi.org/10.3389/fenrg.2022.849064
5. Cheng, Z., Ning, Z., Yu, X., Wang, Q., & Zhang, W. (2019). New insights into spontaneous imbibition in tight oil sandstones with NMR. *Journal of Petroleum Science and Engineering*, *179*, 455–464. https://doi.org/10.1016/j.petrol.2019.04.084
6. Dahi Taleghani, A., Gonzalez-Chavez, M., Yu, H., & Asala, H. (2018). Numerical simulation of hydraulic fracture propagation in naturally fractured formations using the cohesive zone model. *Journal of Petroleum Science and Engineering*, *165*, 42–57. https://doi.org/10.1016/j.petrol.2018.01.063

7. Dutta, R., Lee, C.-H., Odumabo, S., Ye, P., Walker, S. C., Karpyn, Z. T., & Ayala, L. F. (2012). Quantification of Fracturing Fluid Migration due to Spontaneous Imbibition in Fractured Tight Formations. *SPE Americas Unconventional Resources Conference*, SPE-154939-MS. https://doi.org/10.2118/154939-MS
8. Eltahan, E., Rego, F. B., Yu, W., & Sepehrnoori, K. (2021). Impact of well shut-in after hydraulic-fracture treatments on productivity and recovery of tight oil reservoirs. *Journal of Petroleum Science and Engineering*, *203*, 108592. https://doi.org/10.1016/j.petrol.2021.108592
9. Feng, W., Were, P., Li, M., Hou, Z., & Zhou, L. (2016). Numerical study on hydraulic fracturing in tight gas formation in consideration of thermal effects and THM coupled processes. *Journal of Petroleum Science and Engineering*, *146*, 241–254. https://doi.org/10.1016/j.petrol.2016.04.033
10. Habibi, A., Binazadeh, M., Dehghanpour, H., Bryan, D., & Uswak, G. (2015). Advances in Understanding Wettability of Tight Oil Formations. *SPE Annual Technical Conference and Exhibition*, D021S017R006. https://doi.org/10.2118/175157-MS
11. Holditch, S. A., & Tschirhart, N. R. (2005). Optimal Stimulation Treatments in Tight Gas Sands. *SPE Annual Technical Conference and Exhibition*, SPE-96104-MS. https://doi.org/10.2118/96104-MS
12. Jefferson, M. (2020). A crude future? COVID-19s challenges for oil demand, supply and prices. *Energy Research & Social Science*, *68*, 101669. https://doi.org/10.1016/j.erss.2020.101669
13. Jiang, H., Ren, Z., Xi, Y., Liu, G., & Li, J. (2024). Analysis of dynamic thermal behaviors for multi-stage hydraulic fracturing treatments in horizontal shale oil and shale gas wells. *Applied Thermal Engineering*, *240*, 122213. https://doi.org/10.1016/j.applthermaleng.2023.122213
14. Kathel, P., & Mohanty, K. K. (2013). Wettability Alteration in a Tight Oil Reservoir. *Energy & Fuels*, *27*(11), 6460–6468. https://doi.org/10.1021/ef4012752
15. Khan, A. S., Siddiqui, A. R., Abd, A. S., & Alyafei, N. (2018). Guidelines for Numerically Modeling Co- and Counter-current Spontaneous Imbibition. *Transport in Porous Media*, *124*(3), 743–766. https://doi.org/10.1007/s11242-018-1093-3

16. Kilian, L. (2016). The Impact of the Shale Oil Revolution on U.S. Oil and Gasoline Prices. *Review of Environmental Economics and Policy*, *10*(2), 185–205. https://doi.org/10.1093/reep/rew001
17. Kleit, A., & Taleghani, A. D. (2022). COVID Shut-In Choices Across Unconventional Reservoirs: Evidence From the Bakken and the Marcellus. *Journal of Energy Resources Technology*, *144*(7), 073009. https://doi.org/10.1115/1.4054177
18. Li, Z., Qu, X., Liu, W., Lei, Q., Sun, H., & He, Y. (2015). Development modes of Triassic Yanchang Formation Chang 7 Member tight oil in Ordos Basin, NW China. *Petroleum Exploration and Development*, *42*(2), 241–246. https://doi.org/10.1016/S1876-3804(15)30011-2
19. Makhanov, K., Habibi, A., Dehghanpour, H., & Kuru, E. (2014). Liquid uptake of gas shales: A workflow to estimate water loss during shut-in periods after fracturing operations. *Journal of Unconventional Oil and Gas Resources*, *7*, 22–32. https://doi.org/10.1016/j.juogr.2014.04.001
20. Manrique, E., Thomas, C., Ravikiran, R., Izadi, M., Lantz, M., Romero, J., & Alvarado, V. (2010). EOR: Current Status and Opportunities. *SPE Improved Oil Recovery Symposium*, SPE-130113-MS. https://doi.org/10.2118/130113-MS
21. Pan, H., Firoozabadi, A., & Fotland, P. (1997). Pressure and Composition Effect on Wax Precipitation: Experimental Data and Model Results. *SPE Production & Facilities*, *12*(04), 250–258. https://doi.org/10.2118/36740-PA
22. Sandyga, M. S., Struchkov, I. A., & Rogachev, M. K. (2020). Formation damage induced by wax deposition: Laboratory investigations and modeling. *Journal of Petroleum Exploration and Production Technology*, *10*(6), 2541–2558. https://doi.org/10.1007/s13202-020-00924-2
23. Song, C., & Yang, D. (2013). Performance Evaluation of CO2 Huff-n-puff Processes in Tight Oil Formations. *SPE Unconventional Resources Conference Canada*, SPE-167217-MS. https://doi.org/10.2118/167217-MS
24. Sun, Y., Li, Q., Chang, C., Wang, X., & Yang, X. (2022). NMR-Based Shale Core Imbibition Performance Study. *Energies*, *15*(17), 6319. https://doi.org/10.3390/en15176319

25. Teklu, T. W., Zhou, Z., Li, X., & Abass, H. (2016). Experimental Investigation on Permeability and Porosity Hysteresis in Low-Permeability Formations. *SPE Low Perm Symposium*, SPE-180226-MS. https://doi.org/10.2118/180226-MS
26. Thomas, A., Kumar, A., Rodrigues, K., Sinclair, R., Lackie, C., Galipeault, A., & Blair, M. (2014). Understanding Water Flood Response in Tight Oil Formations: A Case Study of the Lower Shaunavon. *SPE/CSUR Unconventional Resources Conference – Canada*, D011S004R001. https://doi.org/10.2118/171671-MS
27. Wang, D., Butler, R., Zhang, J., & Seright, R. (2012). Wettability Survey in Bakken Shale Using Surfactant Formulation Imbibition. *SPE Improved Oil Recovery Symposium*, SPE-153853-MS. https://doi.org/10.2118/153853-MS
28. Wang, F., Ruan, Y., Chen, Q., & Zhang, S. (2021). A pressure drop model of post-fracturing shut-in considering the effect of fracturing-fluid imbibition and oil replacement. *Petroleum Exploration and Development*, *48*(6), 1440–1449. https://doi.org/10.1016/S1876-3804(21)60300-2
29. Wang, J., Liu, H., Zhang, J., Meng, Q., Liu, H., Ge, L., Zhu, Z., & Liu, C. (2018). Experimental investigation on water flooding and continued EOR techniques in buried-hill metamorphic fractured reservoirs. *Journal of Petroleum Science and Engineering*, *171*, 529–541. https://doi.org/10.1016/j.petrol.2018.07.051
30. Wang, J., Liu, H.-Q., Qian, G.-B., & Peng, Y.-C. (2021). Mechanisms and capacity of high-pressure soaking after hydraulic fracturing in tight/shale oil reservoirs. *Petroleum Science*, *18*(2), 546–564. https://doi.org/10.1007/s12182-020-00524-z
31. Yan, Q., Lemanski, C., Karpyn, Z. T., & Ayala, L. F. (2015). Experimental investigation of shale gas production impairment due to fracturing fluid migration during shut-in time. *Journal of Natural Gas Science and Engineering*, *24*, 99–105. https://doi.org/10.1016/j.jngse.2015.03.017
32. Yang, L., Wang, S., Cai, J., Gan, Y., & Salama, A. (2018). Main controlling factors of fracturing fluid imbibition in shale fracture network. *Capillarity*, *1*(1), 1–10. https://doi.org/10.26804/capi.2018.01.01
33. Yang, S., Lai, F., Li, Z., Fu, Y., Wang, K., Zhang, L., & Liang, Y. (2019). The Effect of Temperature on Flowback Data Analysis in Shale Gas Reservoirs: A Simulation-Based Study. *Energies*, *12*(19), 3751. https://doi.org/10.3390/en12193751

34. Yue, M., Zhang, Q., Zhu, W., Zhang, L., Song, H., & Li, J. (2020). Effects of proppant distribution in fracture networks on horizontal well performance. *Journal of Petroleum Science and Engineering*, *187*, 106816. https://doi.org/10.1016/j.petrol.2019.106816
35. Zhang, Q., Liu, W., Wei, J., Taleghani, A. D., Sun, H., & Wang, D. (2022). Numerical Simulation Study on Temporary Well Shut-In Methods in the Development of Shale Oil Reservoirs. *Energies*, *15*(23), 9161. https://doi.org/10.3390/en15239161
36. Zhang, Q., Zhu, W., Liu, W., Yue, M., & Song, H. (2020). Numerical simulation of fractured vertical well in low-permeable oil reservoir with proppant distribution in hydraulic fracture. *Journal of Petroleum Science and Engineering*, *195*, 107587. https://doi.org/10.1016/j.petrol.2020.107587
37. Zhang, Y., Ge, H., Shen, Y., Jia, L., & Wang, J. (2020). Evaluating the potential for oil recovery by imbibition and time-delay effect in tight reservoirs during shut-in. *Journal of Petroleum Science and Engineering*, *184*, 106557. https://doi.org/10.1016/j.petrol.2019.106557
38. Zhao, Y., Liu, L., Zhang, L., Zhang, X., & Li, B. (2019). Simulation of a multistage fractured horizontal well in a tight oil reservoir using an embedded discrete fracture model. *Energy Science & Engineering*, *7*(5), 1485–1503. https://doi.org/10.1002/ese3.379
39. Zhou, Z., Wei, S., Lu, R., & Li, X. (2020). Numerical Study on the Effects of Imbibition on Gas Production and Shut-In Time Optimization in Woodford Shale Formation. *Energies*, *13*(12), 3222. https://doi.org/10.3390/en13123222